ChemComm

Exploring Reaction Dynamics in Lithium-Sulfur Batteries by Time-resolved Operando Sulfur K-edge X-ray Absorption Spectroscopy

Journal:	*ChemComm*
Manuscript ID	CC-COM-01-2019-000485.R1
Article Type:	Communication

COMMUNICATION

Exploring Reaction Dynamics in Lithium-sulfur Batteries by Time-resolved *Operando* Sulfur K-edge X-ray Absorption Spectroscopy

Received 00th January 20xx,
Accepted 00th January 20xx

DOI: 10.1039/x0xx00000x

Enyue Zhao,[a, b, f] Junyang Wang,[a, b, f] Feng Li,*[c] Zheng Jiang,[e] Xiao-Qing Yang,[d] Fangwei Wang,*[a, b, f] Hong Li[a, b, f] and Xiqian Yu*[a, b, f]

A time-resolved *operando* X-ray absorption spectroscopy experiment was successfully designed to explore the sulfur reaction dynamics in lithium-sulfur (Li-S) batteries. It presents directly real-time experiment evidence for the distinct sulfur dynamics at different discharging rates, deepening the understanding of reaction mechanisms for Li-S batteries.

Lithium-sulfur (Li-S) batteries have attracted remarkable attention due to their numerous desirable characteristics for energy storage, such as low cost, high gravimetric energy density (2600 Wh/kg).[1-3] However, the charging efficiency, energy density, rate capability and cycle life of current Li-S batteries can still not meet the requirements for large-scale practical application.[4-6] The issues on Li-S systems are mainly focused on (1) the poor electrical conductivity of S cathode as well as its large volume expansion upon cycling,[7,8] and (2) side-effects (e.g., "shuttle effect",[9,10] lithium corrosion,[11]) originated from the soluble Li polysulfides (i.e., Li_2S_x, $2 < x < 8$). The former challenges have been basically solved by designing electroconductive composite electrodes and suitable cell structures.[12-15] For the latter issues, although strategies by optimizing electrolyte, separator and Li anode have been proved effective, they have not been solved fundamentally due to their intrinsic complexity.[16-21] In-depth understanding the evolution of Li polysulfide and conversion of S cathode upon electrochemical cycling process is significant for tackling the root cause and further advancing the development of Li-S batteries.

a. Beijing National Laboratory for Condensed Matter Physics, Institute of Physics, Chinese Academy of Sciences, Beijing 100190, China. Email: xyu@iphy.ac.cn; fwwang@iphy.ac.cn.
b. Center of Materials Science and Optoelectronics Engineering, College of Materials Science and Opto-Electronic Technology, University of Chinese Academy of Sciences, 100049 Beijing, China.
c. Advanced Carbon Division, Shenyang National Laboratory for Materials Science, Institute of Metal Research, Chinese Academy of Sciences, Shenyang 110016, Liaoning, China. Email: fli@imr.ac.cn.
d. Chemistry Division, Brookhaven National Laboratory, Upton, NY11973, United States.
e. Shanghai Synchrotron Radiation Facility, Shanghai Institute of Applied Physics, Chinese Academy of Sciences, 201204, Shanghai, China.
f. Songshan Lake Materials Laboratory, Dongguan, Guangdong 523808, China.
† Electronic Supplementary Information (ESI) available. See DOI: 10.1039/x0xx00000x

Considering the continuity of electrochemical reactions and high sensitivity of S products to moisture, *in-situ*/*operando* characterization techniques are suitable for studying the S redox reactions and evolution of S products in Li-S batteries.[22-30] Over the past decades, various *in situ*/*operando* techniques, such as X-ray diffraction (XRD), scanning electron microscopy (SEM), transmission X-ray microscopy (TXM), X-ray fluorescence (XRF), Raman, nuclear magnetic resonance (NMR), electron paramagnetic resonance (EPR), resonant inelastic X-ray scattering (RIXS), Fourier transform infrared spectroscopy (FTIR), ultraviolet-visible spectroscopy (UV-vis) and X-ray absorption spectroscopy (XAS), have tremendously promoted the understanding of basic mechanisms in Li-S systems.[22-30] Specifically, the determination of S species, understanding of the S redox chemistry, elucidation of the charging-discharging mechanism, and etc., have been made great progress.[7,31,32] However, most of these *in situ*/*operando* techniques provided the insightful mechanism understanding for Li-S batteries simultaneously with electrochemical cycling at a relative low rate (Fig. S2, ESI†).[24] It is well known that the polysulfide reaction dynamics at high charging/discharging rates is different from that at low rates.[11] Take an example of research conducted by Zheng et al., they found that the Coulombic efficiency (CE) of S/C cathode significantly increase with the elevation of charging/discharging rates.[33] They suggested that this phenomenon should be ascribed to the formation of reduced amount of irreversible Li_2S on the cathode at elevated current densities. In addition, the mechanism information with directly experimental evidences for Li-S systems at high charging/discharging rates, till now, are rarely reported. Nevertheless, it should be noted that understanding the S redox chemistry at high charging/discharging rates is of importance for the in-depth understanding of Li-S mechanisms, especially for the design of cells with high-rate capability.

In this work, we explore the Li-S mechanisms, mainly focusing on the S dynamic behaviours, at various rates (1/8 C, 1/2 C and 2 C, 1 C = 1672 mA g-1) by a time-resolved *operando* XAS technique. It was found that the electrochemical reaction depth of the S cathode is obviously affected by the charging/discharging rates. The formation of Li polysulfides and Li_2S are kinetic-determining reaction steps upon the

discharging process in Li-S batteries. This directly real-time experiment evidence for the distinct sulfur reaction dynamics at different rates in Li-S systems was for the first time provided. The research, on the one hand, deepens and enriches the understanding of the S behaviours in Li-S batteries at different rates, especially at high rates, providing guidance for the design of Li-S cells with high-rate capability; On the other hand, it emphasizes the importance and opens the way to develop highly time-resolved in *situ/operando* characterization techniques.

Compared with other characterization techniques, XAS is sensitive to the oxidation state, chemical environment, type of bonding and site symmetry of the probing element, and capable of detecting species no matter are crystallized or amorphous.[31] Accordingly, XAS technique is a powerful tool to study the Li-S mechanisms, such as S redox chemistry, evolution of S species.[24,28,30] Due to the low absorption energy of S K-edge (2472 eV), it is challenging to perform *operando* XAS measurement and the in situ cell has to be specially made. The *operando* experiment schematic is shown in Fig. 1a, in which a 2 × 1 mm^2 hole sealed by a thin polyethylene film (8 μm) on the cathode side is used to allow X-ray beam penetration.

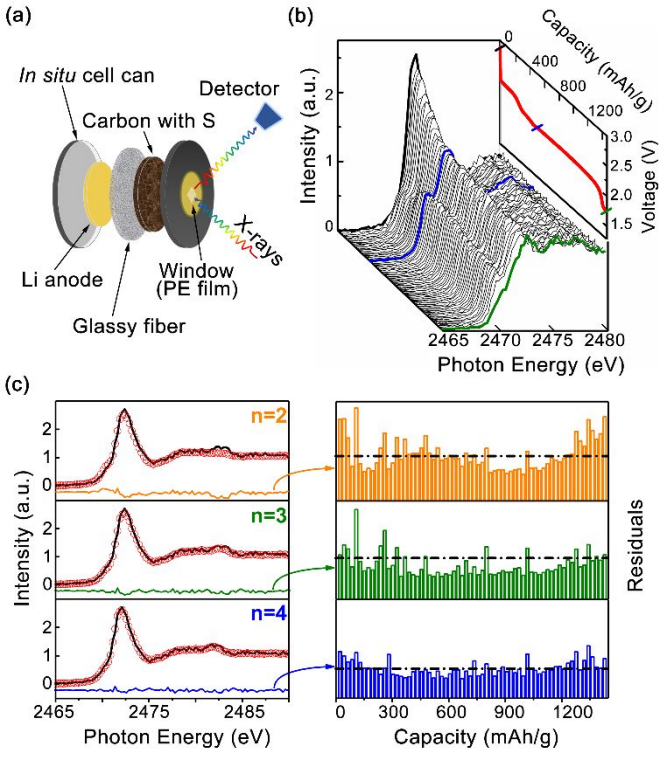

Fig. 1 (a) Schematic of the *in situ* coin cell for simultaneous electrochemical cycling and XAS measurement; (b) S K-edge XAS spectra of the S cathode collected simultaneously with electrochemical cycling at 1/8 C during the first discharging process; (c) PCA results of the S K-edge XAS spectra at the end of the discharged state, in which two (n=2), three (n=3), and four (n=4) principal components were used to fit the spectra, respectively.

Fig. 1b shows the *operando* S K-edge XAS spectra of the S cathode collected simultaneously with electrochemical cycling at 1/8 C rate during the first discharging process. A discharge capacity of ~1500 mA h/g was achieved at this slower rate. According to the previous literature, the XAS feature peak of α-S_8 is located at 2472.2 eV, which is assigned to the high-intensity "white line" (1s to 3p transition) of element S.[31,34] For the Li polysulfide, in addition to the main feature peak at 2472.2 eV, the typical pre-edge located at 2470.5 eV also belongs to their feature peaks, which is ascribed to the terminal S atoms (at the end of polysulfide dianion chains). The main feature of Li_2S XAS peak is usually located at ~2473.2 and ~2475.7 eV, respectively.[28,35] In the following analysis of the *operando* S K-edge XAS spectra, the evolution of Li polysulfide and Li_2S will be identified by the variation of these pre-edge feature peaks. During the entire discharging process, the evolution results of α-S_8 and Li polysulfide can be obtained according to the change of the relative peak intensity at 2472.2 eV and 2470.5 eV (Fig. 1b). A sharp drop of α-S_8 is observed in the high voltage plateau (~2.3 V) concomitantly with the appearance of Li polysulfide. Next, the quantity of Li polysulfide drops gradually during the subsequent discharging process (~2.1V) together with the formation of crystalline Li_2S.

Limited by the lack of XAS spectra of reference materials (difficulties to obtain pure polysulfide LixS8 species), in principle, it is unable to quantitatively resolve the spectra.[25,30] Herein, a purely mathematic (regardless of the physical mode) analysis method, namely principal components analysis (PCA), was used to qualitatively identify the amounts of terminal S species during the discharging process. The PCA results of the S K-edge XAS spectra at the end of the discharging process was shown in Fig. 1c. It can be seen that the error bar was very uneven when two assumed principal components were used to fit the spectra, and the error bar levelled off with the increase of the principal components. Overall, it can be concluded that more than three or four S species with distinct XAS feature exist during the entire discharging process. Meanwhile, the complexity of the S cathode redox reactions can be reflected in this result.

In order to further explore the real-time S reaction dynamic behaviour at different rates, especially at high rates, time-resolved *operando* XAS technique was performed at the discharge rate of 1/2 C and 2 C, respectively (Fig. S3 and S4, ESI†). As mentioned above, the variation of shoulder XAS peak located at 2470.5 eV (denoted as P1) and main XAS peak located at 2472.2 eV (denoted as P2) can be used to directly reveal the chemical-composition evolution of S cathode upon the electrochemical cycling process. For instance, as shown in Fig. 2a, from the electrochemical state "a" to "c" (i.e., at the high voltage plateau of about 2.3 V), the intensity of P1 and P2 increases and decreases, respectively, which represents the conversion of α-S_8 to long-chain Li polysulfides. From the electrochemical state "c" to "d" (i.e., at the low voltage plateau of about 2.1 V), the intensity of P1 decreases and the location of P2 shifts to higher energy, indicating the conversion of soluble Li polysulfides to insoluble Li_2S_2 and Li_2S. The intensity and location evolution results of P1 and P2 upon the overall discharging process at different rates are shown in Fig. 2b and Fig. S5, respectively. It can be seen that there is an obvious location shift of P1/P2 (highlighted by red and blue

shadow in Fig. S5, ESI†) and intensity decrease of P1 (indicated by blue arrow in Fig. 2b) from the state "c" to "d" at 1/8 C. The similar evolution results were not observed at 1/2 C and 2C. In the meantime, the feature peaks of Li_2S located at ~2473.2 and ~2475.7 eV are also difficult to detected at high rates (highlighted by yellow shadow in Fig. S5, ESI†). This discrepant evolution of P1 and P2 at different discharging rates suggests that the conversion process of long-chain Li polysulfides to insoluble Li_2S_2 and Li_2S is a kinetic-determining reaction step.

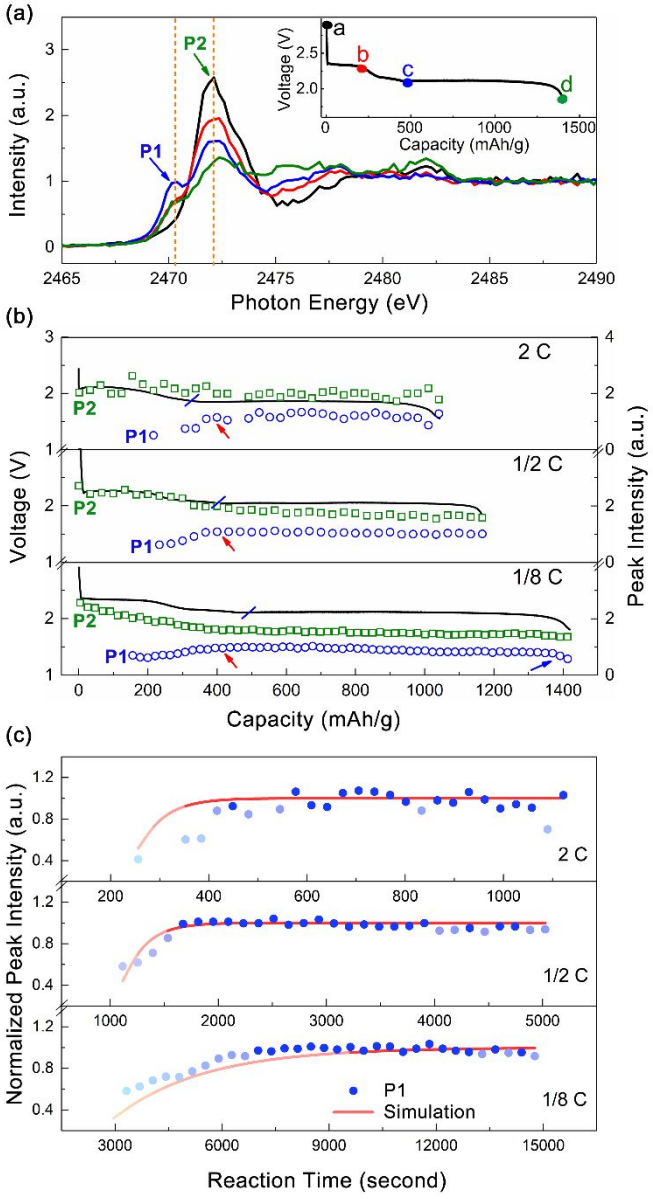

Fig. 2 (a) S K-edge XAS spectra of different discharged states at the discharging rate of 1/8 C; (b) The evolution of peak 1 (P1) and peak 2 (P2) upon the discharging process at different discharging rates, in which red arrows indicate the stopping of the intensity growth of P1. The high voltage plateau of the discharging curve is shown by blue bars; (c) The comparison of the growth of P1 intensity and simulated electrochemical reaction process of Li polysulfides formation at different electrochemical rates. The deep colour in blue dots and red line represents the termination of Li polysulfides formation and electrochemical reaction of α-S_8 into long-chain polysulfides, respectively.

In addition, the obviously different intensity evolution results of P2 at different rates at high voltage plateau (shown by olive block in Fig. 2b) indicates that the conversion process of α-S_8 to Li polysulfides is closely correlated with the discharging rate. Considering P_2 is the feature peak of both α-S_8 and Li polysulfides and its intensity variation would be disturbed by this factor, thus, we further focused on the detailed evolution of P1 to clarify the effect of discharging rate on the conversion process of α-S_8 to Li polysulfides. It has been reported that the conversion of α-S_8 to Li polysulfides mainly occurs at the high voltage plateau at 2.3 V, and the process of which will be accompanied by the intensity increase of P1. Obviously, the intensity growth of P1 stops later or earlier than the electrochemical reaction step at 2 C and 1/8 C, respectively, while the intensity growth of P1 and electrochemical reaction step almost simultaneously stop at the rate of 1/2 C (indicated by red arrows and blue bars in Fig. 2b). This phenomenon undoubtedly revealed that the conversion of α-S_8 to long-chain Li polysulfides is a kinetic-determining process, even at a moderate discharge rate of 2C, which is usually not taken into consideration in previous researches.[29,32,33,36] The quantitative analysis of this conversion process further demonstrates the above conclusion. Specifically, as shown in Fig. 2c, based on a simplified electrochemical reaction model, the formation step of Li polysulfides can be simulated with the specific electrochemical process at different discharging rates. The calculated formation reaction rate coefficients (k) are 0.0004/s, 0.005/s and 0.02/s at the discharging rate of 1/8 C, 1/2 C, and 2 C, respectively, demonstrating that the theoretical formation rate of Li polysulfides will enhance with the increase of discharging rate (Fig. S1, ESI†). After comparing the theoretical formation rate of Li polysulfides (red line in Fig. 2c) with its practical formation rate (blue dot in Fig. 2c), it can be summarized that the practical formation rate of Li polysulfides is lower or higher than the theoretical formation rate at 2 C and 1/8 C, respectively, while the practical formation rate of Li polysulfides is almost similar with its theoretical value at the rate of 1/2 C.

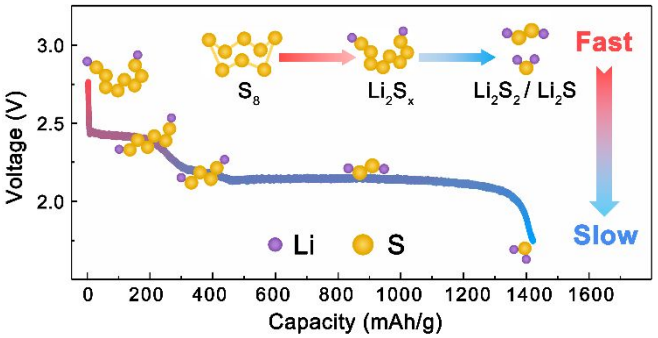

Fig. 3 Proposed multistep kinetic-determining reaction steps upon the first discharging process in Li-S batteries.

Overall, it can be concluded that the discharging rate can directly affect the dynamic behaviour of S cathode and electrochemical reaction depth. Li-S batteries show different electrochemical and chemical equilibrium states at high rate

compared with that at low rate. As shown in Fig. 3, the intermediate multistep conversion reactions from α-S_8 to Li_2S are kinetic-determining process. Specifically, the conversion process from α-S_8 to long-chain soluble polysulfides Li_2S_x, long-chain soluble polysulfides Li_2S_x to short-chain Li_2S_2 and Li_2S are directly correlated with the discharging rates. The *operando* XAS experiment operated at different discharging rates provided directly real-time experiment evidence for the multistep kinetic-determining conversion reactions in Li-S batteries, especially for the reaction step of α-S_8 to long-chain soluble polysulfides.

In conclusion, a time-resolved operando XAS experiment operated at different discharging rates was successfully designed. The experiment results suggest that the S dynamic behaviour and electrochemical reaction steps can be significantly affected by the discharging rate. The highly time-resolved operando XAS provided directly real-time experiment evidence for the multistep kinetic-determining reaction steps in Li-S systems upon the first discharging process. This work highlights the importance of the highly time-resolved *operando* techniques in deepening the reaction mechanism for Li-S batteries.

This work is supported by the National Key R&D Program of China (2016YFA0401503), National Materials Genome Project (2016YFB0100106), NSFC (Grant No. 11675255, 51502334, 51822211). The work at BNL was supported by the Assistant Secretary for Energy Efficiency and Renewable Energy, Vehicle Technology Office of the U.S. DOE through the Advanced Battery Materials Research (BMR) Program, including Battery500 Consortium under Contract DE-SC0012704. The authors acknowledge Dr. Jie Xiao and Dr. Huilin Pan from Pacific Northwest National Laboratory for providing the experimental samples.

Conflicts of interest

There are no conflicts to declare.

Notes and references

1 A. Manthiram, Y. Fu, S.-H. Chung, C. Zu and Y.-S. Su, *Chem. Rev.*, 2014, **114**, 11751.
2 A. Manthiram, S.-H. Chung and C. Zu, *Adv. Mater.*, 2015, **27**, 1980.
3 Z. W. Seh, Y. Sun, Q. Zhang and Y. Cui, *Chem. Soc. Rev.*, 2016, **45**, 5605.
4 A. Manthiram, Y. Fu and Y.-S. Su, *Acc. Chem. Res.*, 2013, **46**, 1125.
5 R. Fang, S. Zhao, Z. Sun, W. Wang, H.-M. Cheng and F. Li, *Adv. Mater.*, 2017, **29**.
6 6 X. Ji, K. T. Lee and L. F. Nazar, *Nat. Mater.*, 2009, **8**, 500.
7 7 J. Liang, Z.-H. Sun, F. Li and H.-M. Cheng, *Energy Storage Materials*, 2016, **2**, 76.
8 8 S. Doerfler, M. Hagen, H. Althues, J. Tuebke, S. Kaskel and M. J. Hoffmann, *Chem. Commun.*, 2012, **48**, 4097.
9 9 J. Liang, L. C. Yin, X. N. Tang, H. C. Yang, W. S. Yan, L. Song, H. M. Cheng and F. Li, *ACS Appl. Mat. Interfaces*, 2016, **8**, 25193.
10 10 R. Fang, S. Zhao, Z. Sun, D.-W. Wang, R. Amal, S. Wang, H.-M. Cheng and F. Li, *Energy Storage Materials*, 2018, **10**, 56.
11 M. Wild, L. O'Neill, T. Zhang, R. Purkayastha, G. Minton, M. Marinescu and G. J. Offer, *Energy Environ. Sci.*, 2015, **8**, 3477.
12 N. Jayaprakash, J. Shen, S. S. Moganty, A. Corona and L. A. Archer, *Angew. Chem. Int. Ed.*, 2011, **50**, 5904.
13 N. Li, M. Zheng, H. Lu, Z. Hu, C. Shen, X. Chang, G. Ji, J. Cao and Y. Shi, *Chem. Commun.*, 2012, **48**, 4106.
14 J.-Q. Huang, Q. Zhang, H.-J. Peng, X.-Y. Liu, W.-Z. Qian and F. Wei, *Energy Environ. Sci.*, 2014, **7**, 347.
15 L. Li, G. M. Zhou, L. C. Yin, N. Koratkar, F. Li and H. M. Cheng, *Carbon*, 2016, **108**, 120.
16 T. Tao, S. Lu, Y. Fan, W. Lei, S. Huang and Y. Chen, *Adv. Mater.*, 2017, **29**.
17 Z. Wang, Y. Dong, H. Li, Z. Zhao, H. B. Wu, C. Hao, S. Liu, J. Qiu and X. W. Lou, *Nat. Commun.*, 2014, **5**.
18 Z. H. Sun, J. Q. Zhang, L. C. Yin, G. J. Hu, R. P. Fang, H. M. Cheng and F. Li, *Nat. Commun.*, 2017, **8**.
19 D.-W. Wang, Q. Zeng, G. Zhou, L. Yin, F. Li, H.-M. Cheng, I. R. Gentle and G. Q. M. Lu, *J. Mater. Chem. A*, 2013, **1**, 9382.
20 G. Zhou, L. Li, D.-W. Wang, X.-y. Shan, S. Pei, F. Li and H.-M. Cheng, *Adv. Mater.*, 2015, **27**, 641.
21 Y.-S. Su and A. Manthiram, *Chem. Commun.*, 2012, **48**, 8817.
22 S.-M. Bak, Z. Shadike, R. Lin, X. Yu and X.-Q. Yang, *NPG Asia Materials*, 2018, **10**, 563.
23 F. Lin, Y. Liu, X. Yu, L. Cheng, A. Singer, O. G. Shpyrko, H. L. Xin, N. Tamura, C. Tian, T.-C. Weng, X.-Q. Yang, Y. S. Meng, D. Nordlund, W. Yang and M. M. Doeff, *Chem. Rev.*, 2017, **117**, 13123.
24 J. Tan, D. Liu, X. Xu and L. Mai, *Nanoscale*, 2017, **9**, 19001.
25 E. Zhao, K. Nie, X. Yu, Y.-S. Hu, F. Wang, J. Xiao, H. Li and X. Huang, *Adv. Funct. Mater.*, 2018, **28**, 1707543.
26 M. A. Lowe, J. Gao and H. D. Abruna, *RSC Adv.*, 2014, **4**, 18347.
27 J. Nelson, S. Misra, Y. Yang, A. Jackson, Y. Liu, H. Wang, H. Dai, J. C. Andrews, Y. Cui and M. F. Toney, *J. Am. Chem. Soc.*, 2012, **134**, 6337.
28 L. Zhang, D. Sun, J. Feng, E. J. Cairns and J. Guo, *Nano Lett.*, 2017, **17**, 5084.
29 M. Kavcic, K. Bucar, M. Petric, M. Zitnik, I. Arcon, R. Dominko and A. Vizintin, *J. Phys. Chem. C*, 2016, **120**, 24568.
30 K. H. Wujcik, T. A. Pascal, C. D. Pemmaraju, D. Devaux, W. C. Stolte, N. P. Balsara and D. Prendergast, *Adv. Energy Mater.*, 2015, **5**, 1500285.
31 Y. Gorlin, M. U. M. Patel, A. Freiberg, Q. He, M. Piana, M. Tromp and H. A. Gasteiger, *J. Electrochem. Soc.*, 2016, **163**, A930.
32 Z.-Q. Jin, Y.-G. Liu, W.-K. Wang, A.-B. Wang, B.-W. Hu, M. Shen, T. Gao, P.-C. Zhao and Y.-S. Yang, *Energy Storage Materials*, 2018, **14**, 272.
33 J. Zheng, M. Gu, M. J. Wagner, K. A. Hays, X. Li, P. Zuo, C. Wang, J.-G. Zhang, J. Liu and J. Xiao, *J. Electrochem. Soc.*, 2013, **160**, A1624.
34 K. H. Wujcik, D. R. Wang, T. A. Pascal, D. Prendergast and N. P. Balsara, *J. Electrochem. Soc.*, 2017, **164**, A18.
35 K. H. Wujcik, J. Velasco-Velez, C. H. Wu, T. Pascal, A. A. Teran, M. A. Marcus, J. Cabana, J. Guo, D. Prendergast, M. Salmeron and N. P. Balsara, *J. Electrochem. Soc.*, 2014, **161**, A1100.
36 M. Cuisinier, P. E. Cabelguen, B. D. Adams, A. Garsuch, M. Balasubramanian and L. F. Nazar, *Energy Environ. Sci.*, 2014, **7**, 2697.

Table of Contents

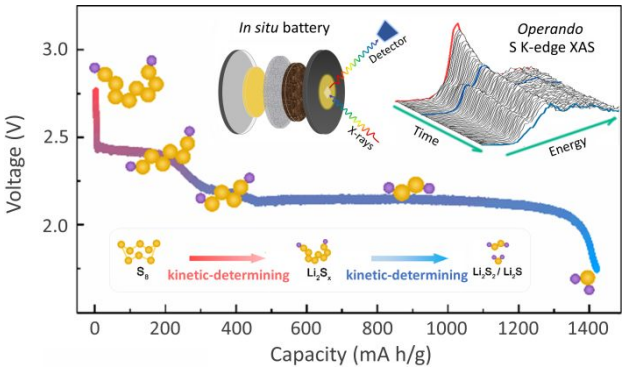

The multistep kinetic-determining conversion process of sulfur electrode is directly revealed through time-resolved *operando* X-ray absorption spectroscopy.